NOTES AND CORRESPONDENCE

Zonal Teleconnections and Longitude–Time Lag Correlations of the 500 mb Geopotential along 50° S

KLAUS FRAEDRICH* AND MARTIN LUTZ

Institut für Meteorologie, Freie Universität Berlin, D-1000 Berlin 41, West Germany

30 September 1985 and 14 March 1986

ABSTRACT

Unfiltered, band- and low-pass filtered geopotential height values of the 500 mb level along 50°S are analyzed to evaluate teleconnections and zonal wave-propagation properties in the Southern Hemisphere (SH) midlatitudes. Correlation matrices of low-pass filtered data illustrate the dominant patterns of hemispheric and regional anomalies: the transpolar teleconnection, the South American anomaly and a stationary wavenumber 3 pattern (with contributions from wavenumbers 2 and 4). Longitude–time lag correlations of the low-pass filtered data document an eastward energy dispersion along a quasi-stationary zonal wave train; it emerges from the area of South America, has a wavelength of 90 to 100° longitude, and a group velocity of ~10° per day. The band-pass filtered correlation matrices for this latitude circle reveal the sectors of the major storm tracks. The related longitude–time lag correlations show a wavelength of 70° to 80° longitude, an eastward propagation of ~10° per day and a group velocity of ~50° per day.

1. Introduction

Zonal time statistics and wavenumber-frequency analyses of the 500 mb geopotential in the midlatitudes of the summer and winter Southern Hemisphere (SH) reveal some interesting features about medium-scale planetary waves: Two separated variance maxima are observed in the wavenumber-frequency spectra of the meridional component of the geostrophic wind which contribute to the transient eddy variance. They occur in the long period range (wavenumber $k \sim 4$–5 and period $p \sim 8$–12 days) and short period range ($k \sim 6$–7, $p \sim 6$ days) of eastward traveling waves with phase speeds $c \sim 6$ m s^{-1} and $c \sim 11$ m s^{-1}, respectively (Fraedrich and Kietzig 1983; based on gridded South African weather maps for five summer and winter seasons 1959–64 along 50°S). Several researchers have shown similar evidence of zonally propagating waves of zonal wavenumber $k \sim 4$–7: Salby (1982; U.S. analyses of 17 December to 17 March 1978/79), Mechoso and Hartmann (1982; U.S. analyses May to September 1979), Hamilton (1983; Australian analyses 1972–79). In particular, Hartmann (1976; Nimbus 5 radiance observations from 1 July to 6 September 1973, Fig. 9a), Randel and Stanford (1983 and 1985a,b; U.S. analyses for one or three summers, December to 28 February during 1978/79 to 1980/81) reproduce basically the same two distinct spectral variance maxima for the longer and shorter medium scale waves from different data sets.

The techniques of wavenumber-frequency analysis are not the best means of studying low frequency ultra-long planetary wave variability because they implicitly assume that there is no temporal coherence between the respective sine and cosine coefficients (Wallace and Hsu, 1983). One alternative approach toward the long period variability is the examination of correlation maps of monthly (or seasonal) means as suggested by Wallace and Gutzler (1981); they analyzed Northern Hemisphere (NH) teleconnections in winter; Mo and White (1985) used the same method to reveal some aspects of hemispheric teleconnections in the Southern Hemisphere (SH). Another approach is the analysis of persistent anomalies defined by geopotential heights exceeding threshold values in magnitude and duration as described by Dole (1983); he applied it to the extra-tropical wintertime circulation of the Northern Hemisphere. Trenberth and Mo (1985) analyzed blocking in the midlatitudes of the SH using basically the same technique.

These analyses of regional low-frequency variability support the concept of Rossby wave phase propagation and energy dispersion whose relevance to atmospheric planetary waves has become widely recognized only recently (e.g., Hoskins et al., 1977). In the Northern Hemisphere the two-dimensional conceptual model of Rossby wave dispersion appears to be applicable with wave trains on great circle route orientations. In the SH midlatitudes, however, zonal propagation and energy dispersion appear to dominate the low frequency variability at least at times. Some results of the studies on SH low frequency variability are briefly described: In midlatitudes the planetary waves display a wavenumber 3 pattern with surprising regularity, in particular in winter; Wallace and Hsu (1983) showed that a stationary zonal wavenumber 3 dominated the 500 mb geopotential height field in the SH from 6 July to 4

* Present affiliation: Bureau of Meteorology Research Centre, Melbourne, Vic. 3001, Australia.

August 1981 (daily ECMWF-analysis) which, they concluded, is suggestive of one-dimensional zonal Rossby wave dispersion in SH midlatitudes. Mo and White (1985) found a striking zonal wavenumber 3 correlation pattern over the Southern Ocean, applying Wallace and Gutzler's (1981) approach of correlating monthly means (Australian 500 mb analyses 1972–80). Trenberth and Mo (1985; using the same but daily Australian analyses) find wavenumber 3 (and wavenumber 6 to a lesser extent) playing a prominent role in SH blocking. They analyzed persistent (≥5 days) height anomalies (following Dole 1983) as averages over the SH midlatitude band from 45° to 62°S where blocking is most frequent. The locations of the blocking areas coincide with the low-frequency variance maxima (Trenberth, 1982, using an 8–64 day period band-pass filter on the 1972–79 Australian analyses) and with the regions of negative skewness along 50°S south of New Zealand, southeast of South America, and to a lesser extent, in the southern Indian Ocean (Fraedrich and Kietzig, 1983; Trenberth and Mo, 1985).

These results suggest that the relevant SH teleconnection patterns which occur in the midlatitudes are related to a zonal energy dispersion by planetary Rossby wave trains. In the following note, we supplement our analyses on wavenumber-frequency spectra along 50°S (Fraedrich and Kietzig, 1983) by evaluating high and low frequency correlation patterns of the 500 mb geopotential along the 50°S latitude circle: (i) to make further use of an uncommon data set; (ii) to study SH midlatitude teleconnections by this independent data set using band- and low-pass filtered correlations (as Blackmon et al., 1983, did for the NH) and not monthly means, and (iii) to present evidence of zonal wave train energy dispersion in the SH by longitude-time lag-correlations along 50°S.

2. Data and method of analysis

This study covers a data set of the 500 mb geopotential height gridded along the 50° latitude circle of the Southern Hemisphere. The data source is given by daily circumpolar 500 mb charts for 1200 GMT of the South African Weather Service, published in *Notos* (1964–1970). These charts are based on all types of available data which can possibly be used for an a posteriori daily synoptic analysis. The procedure of map construction and extrapolation has been described by Taljaard and van Loon (1960, 1964). It appears reasonable to choose the 50°S latitude circle for statistical analyses of the SH midlatitude dynamics because the main storm track is along 50°S, blocking occurs in the latitude band between 40°–60°S, and stationary waves (in particular, wavenumber 3) reveal their maximum amplitude in the midlatitudes. Thus, daily geopotential height charts $z(\lambda, t)$ of the last five summer and winter seasons (1959–64) published by the South African Weather Service are gridded on a 10° longitude grid (λ) around 50°S. The scale of the smallest eddy resolved will be 1500 km. The data sets have an equal length of 120 days beginning on 1 November (summer) and 1 May (winter). Circulation statistics deduced from this data set show general agreement with results obtained from objectively analyzed and more recent observations (see section 1).

The annual cycle is removed from each grid point

$$z(\lambda, t) = \text{removed} + z^*(\lambda, t)$$

by fitting a least-squares parabola to each season's data and then subtracting it. This operation has the effect of removing the climatological cycle, the interannual variability of the seasons and a small part of the very long period variability within the seasons. The remaining deviations $z^*(\lambda, t)$ are statistically analyzed in the following.

a. Filters

To distinguish representative scales, geopotential height anomalies $z^*(\lambda, t)$ are subjected to time filtering before correlation coefficients are derived. Band- and low-pass filters are applied using 31 weighting points which are identical to those in Blackmon (1976). This reduces the unfiltered 120 day season by the first and the last 15 days; i.e., the filtered seasons consist of 90 days. The physical relevance of these filters becomes obvious from wavenumber-frequency spectra of the geopotential height (and meridional geostrophic wind) in the Southern Hemisphere along 50°S (Fraedrich and Kietzig, 1983, Figs. 1 and 2). The band-pass filter responds to periods between 5 and 10 days. This corresponds to eastward propagating waves associated with zonal wavenumbers 5 and 6 representing cyclones (and cyclone families). The low-pass filtered data contain periods longer than 15 days. This covers variance contributed by long propagating waves and the ultra-long periods of the quasi-stationary systems associated with wavenumbers 4 and smaller. These filters are approximately comparable with Trenberth's (1981, 1982) band-pass filters which respond to the periods between 2–8 days, characterizing storm tracks and 8–64 days for blocking type events.

b. Correlation matrix

Correlation coefficients are determined from the height anomalies z^* of zonal grid points at different longitudes λ and $\lambda + m\Delta\lambda$:

$$r_{\lambda,\lambda+m} = \frac{\text{cov}[z^*(\lambda, t), z^*(\lambda + m\Delta\lambda, t)]}{\{[\text{var}z^*(\lambda, t)][\text{var}z^*(\lambda + m\Delta\lambda, t)]\}^{1/2}}.$$

The variances and covariances refer to anomalies in z^*. Thus one obtains for each base point (at λ) a zonal profile of m correlation coefficients, $r_{\lambda,\lambda+m}$. They depend on $m = 0, \ldots, 36$ space steps which are a zonal

distance of $\Delta\lambda = 10°$ longitude apart. The sampling time is $\Delta t = 1$ day. The correlations lead to a symmetric correlation matrix; the elements in the main diagonal are $r_{\lambda,\lambda} = 1$.

c. *Teleconnections*

The correlation matrices of the unfiltered or band-pass filtered data sets reveal troughs and ridges. They are caused by standing and/or propagating oscillations with wavelengths of about twice the distance between a base point at λ (i.e., along the main diagonal) and the location of the minimum (i.e., maximum negative) correlations along the adjacent subdiagonal. Low-pass filtered correlation matrices reveal dipoles. These neighboring pairs of correlation extrema are given by the absolute maximum on the diagonal and the adjacent minimum along the latitude circle and defined as teleconnections.

d. *Circulation index and composites*

A circulation index, say I, can be introduced for each significant teleconnection pattern or correlation dipole. It is defined by a linear combination of normalized 500 mb height anomalies, $\hat{z}$, at the centers of the teleconnection. The normalization is given by seasonal standard deviations of daily geopotential heights. This provides an index for all synoptic situations. Days with both high and low index values are separately composited to represent the teleconnected circulation pattern in terms of zonal geopotential height profiles. More specifically, the composites are produced by those situations $I(t)$, for which the index lies above or below its σ_I-boundary: $I(t) \gtrless I \pm \sigma_I$, with σ_I = variance(I); i.e., about 16% of all days contribute to the composites of both high or low circulation indices. Here it should be noted that low and high index values imply a change of the anomaly in the sense that a persistent dipole-like pattern reverses sign in amplitude but remains stationary.

3. Teleconnections along the 50°S latitude circle

Unfiltered, band- and low-pass filtered correlation matrices are evaluated. To stress dipole or wave-like patterns, only the negative correlations are resolved in detail whereas the positive correlations are left blank. The statistical significance of the correlation coefficients is discussed in the Appendix.

The unfiltered data set reveals longitude correlations which are due to the whole spectrum of large-scale atmospheric dynamics (Fig. 1a, b). The related correlation matrices along the representative latitude circle present the basic structures of these processes. Thus, for a qualitative comparison of the zonality of Northern and Southern Hemisphere dynamics their zonal correlation matrices are combined to a single display of two symmetric half-matrices which have the main di-

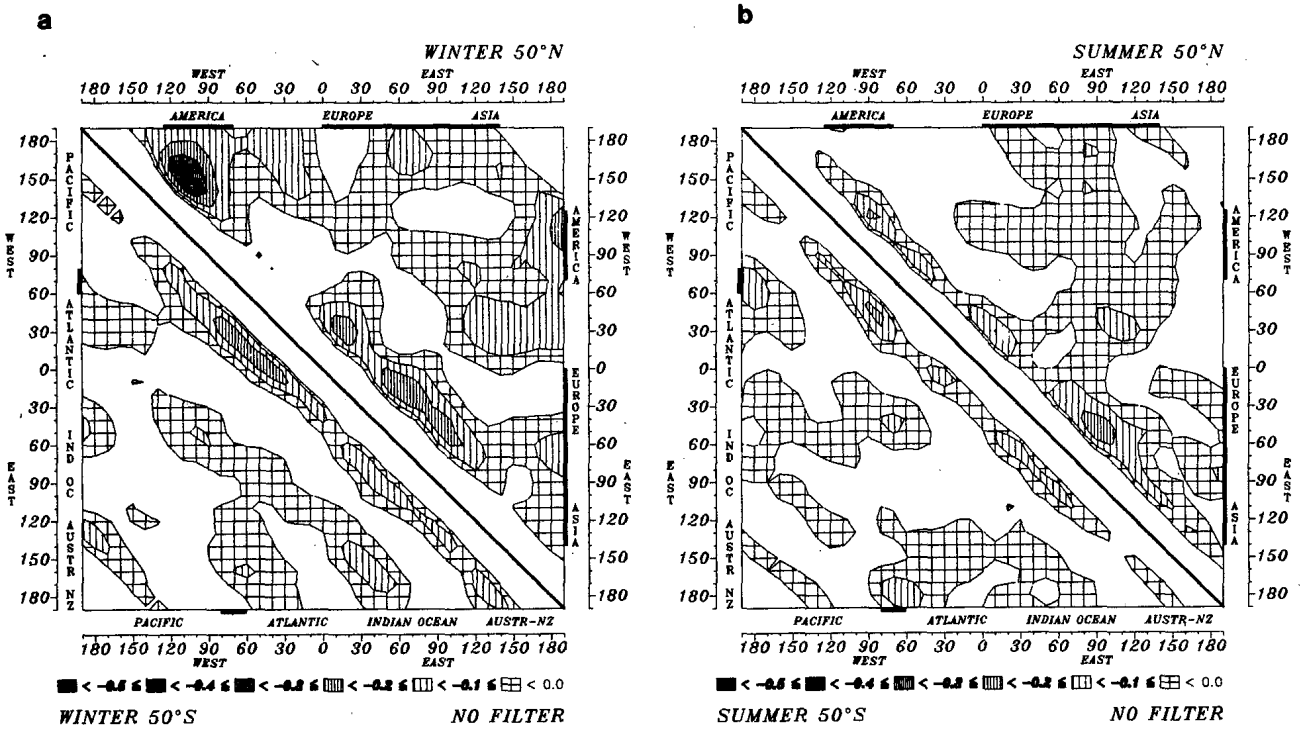

FIG. 1. Correlation matrix of unfiltered 500 mb geopotential height deviations along 50° north and south for (a) winter and (b) summer. Positive correlations are left blank; 95% significance is indicated on the signature scale (thick numbers).

agonal ($r_{\lambda,\lambda} = 1$) in common. They show distinct hemispheric differences: the strong zonality of the SH midlatitudes (lower half-matrix) and the zonal asymmetries of the NH, which are more developed in winter than in summer (upper half-matrix; these data are based on the 500 mb geopotential along 50°N for winter, November through February, and summers, May through August, 1967 to 1982. The data analyzed are digitized from daily hemispheric charts of the Deutscher Wetterdienst). The SH zonality can be inferred from the diagonal orientation of the correlation patterns, which is particularly well established during winter. Almost every grid point shows a similar zonal wave structure when moving horizontally and vertically from the main diagonal in the lower left parts of the diagrams (Fig. 1). This, however, cannot be observed in the Northern Hemisphere (upper right part of the diagrams, Fig. 1); one finds a stronger zonal irregularity associated with large intensity variations of the zonal correlation coefficients (see, for example, the Pacific-North America dipole with centers at 150°W and 100°W on 50°N).

The unfiltered correlation matrices of daily geopotential heights (Fig. 1) show how all scales combined lead to a mixture of patterns, whereas more information is gained by applying both band- *and* low-pass filters to the data set (Fig. 2). Teleconnection dipoles appear as negative correlation maxima in the neighborhood of the main (blank) diagonal of the low-pass filtered correlation half-matrix. Referring to the low-frequency dynamics of the SH winter, for example (Fig. 2a), the base point $\lambda = 90°W$ (on the 50°S latitude circle) has the strongest positive correlation with itself (i.e., $r_{\lambda,\lambda} = 1$ on the main diagonal) and the strongest nearby negative correlation with 40°W. This defines a *South American teleconnection (a)*. It can be visualized when moving to the right from the base point $\lambda = 90°W$ (situated on the main diagonal of the low-pass filtered correlation half-matrix, Fig. 2a). Furthermore, $\lambda = 40°W$ on the diagonal is negatively correlated with 150°E (moving to the right in the correlation half-matrix); this leads to a long-distance *transpolar teleconnection (b)*. Winter teleconnections are discussed in more detail than summer anomalies (c), because both low-pass filtered correlation patterns (a) and (b) are significant only during winter. (See Fig. 2, summer and winter correlation matrices for low-pass filtered geopotentials.)

Composites can be constructed from daily 500 mb geopotential height fields (section 2). They are associated with low and high circulation indices defined by (a) the South American pattern and (b) the transpolar teleconnection (Fig. 3). The Indian Ocean link contributes to both, as suggested by the second hemispheric eigenvector of daily 500 mb maps (Rogers and van

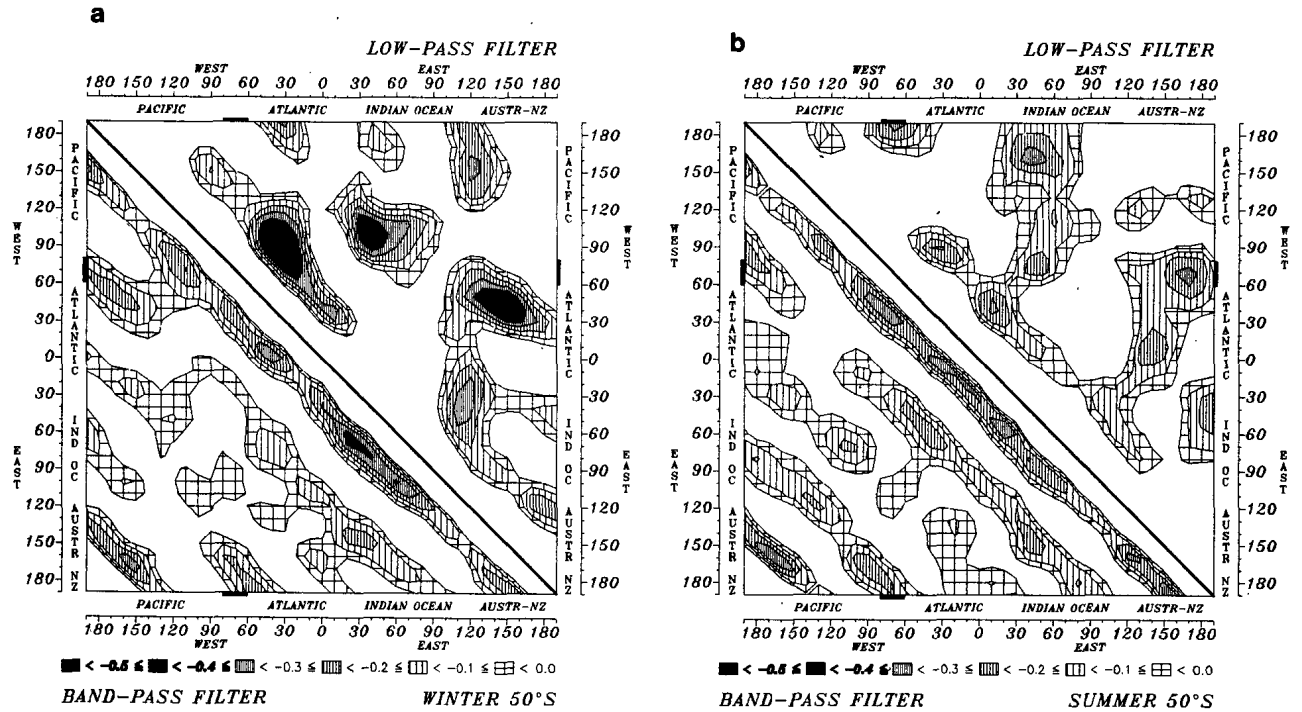

FIG. 2. Correlation matrix of band- and low-pass filtered 500 mb geopotential height deviations along 50°S for (a) winter and (b) summer. Positive correlations are left blank; 95% significance is indicated on signature scale. (See text.) The centers of minimum (maximum negative) correlations (dark signature) refer to predominant teleconnections (anomalies) where related longitudes define a pattern. Low-pass filtered data (upper right part) present persistent anomalies across South America (90°W, 40°W), a transpolar teleconnection (40°W, 150°E), and a wavenumber 3 pattern (150°W, 40°W, 40°E). The Indian Ocean–South African correlation is related to both South America and transpolar anomalies. Band-pass filtered data (lower left part) refer to storm tracks.

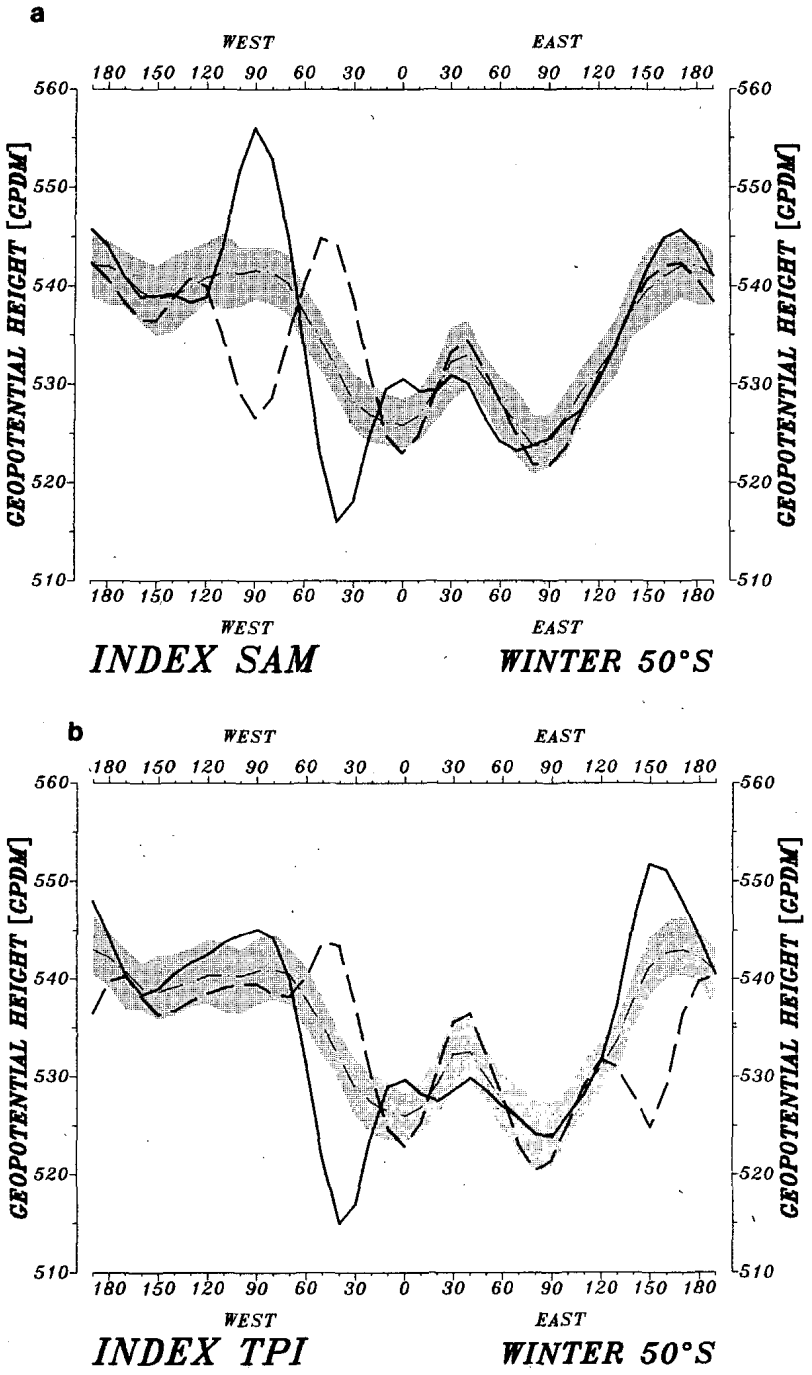

FIG. 3. Composite geopotential height profiles of persistent anomalies along 50°S during winter refer to high (full line) and low (full dashed) index values; the remaining data lead to a mean profile (thin dashed line). The shaded area denotes the confidence interval from which high and low index profiles deviate. From top to bottom: (a) South America and (b) transpolar teleconnection.

Loon, 1982). The statistical significance of the composited zonal height profiles (Fig. 3, thick full and dashed lines refer to maximum and minimum index) can be deduced by comparing them with the zonal height profiles obtained by averaging over the remaining days which account for about 68% of data (Fig. 3, thin dashed line). Using the nonparametric rank sum test of Mann and Whitney (1947; see also Bradley, 1968) by steps, a confidence interval can be computed around the mean which is composited by the remaining data. This allows one to test whether the composites of high and low index values are significantly different

from this residual mean. This test has been chosen, because there are no constraints on the distribution of the populations.

a. South America

The South America teleconnection presents a geopotential height dipole (or wave) with centers over the eastern South Pacific (90°W) and western South Atlantic (40°W), which appears in both the unfiltered and low-pass filtered correlation matrix. Both centers are separated by the Andes which are the only significant barrier to the SH westerlies. The following index refers to the base point at 90°W:

$$\mathrm{SAM} = \tfrac{1}{2}\hat{z}\,(90°\mathrm{W}) - \tfrac{1}{2}\hat{z}\,(40°\mathrm{W}),$$

which is related to the other steering center at 40°W. Positive (negative) values require high (low) geopotential heights in the eastern South Pacific and low (high) geopotentials in the South Atlantic; i.e. if there is blocking action in the South Atlantic area the SAM index is negative. The composites (Fig. 3a) of extremal indices stress the SAM-dipole pattern. Impacts on the Indian Ocean (30°E to 60°E) and, to a lesser extent, on the Australian-New Zealand region (120°E to 150°E) may also be noticed, but they are not significant.

b. Trans-Polar

This pattern (TPI after Pittock, 1980, 1984) appears in the low-pass filtered data set connecting Australia with South America and the South Atlantic. The related circulation index has been originally defined as the surface pressure anomaly at Hobart (43°S, 147°E) minus that at Stanley (52°S, 58°W). Here we shall consider (Fig. 3b)

$$\mathrm{TPI} = \tfrac{1}{2}\hat{z}\,(150°\mathrm{E}) - \tfrac{1}{2}\hat{z}\,(40°\mathrm{W}).$$

Pittock (1980) states that this pattern "represents an eccentricity of the polar vortex about the South Pole with a tendency for the vortex to be preferentially displaced either towards South America and the South Atlantic or Australia-New Zealand." The composites illustrate this anomaly as a wavenumber 1 phenomenon (Fig. 3b). Furthermore, global-scale studies of precipitation find coherent patterns of variations which in the SH include simultaneous anomalies over southern Africa, Australia and New Zealand, South America (Pittock, 1984). The South African-Indian Ocean correlation minimum in winter (Fig. 2a, 30° to 60°E) will not be investigated as a distinct teleconnection pattern; it seems to be related with both the Trans-Polar and South American teleconnections. This is partly confirmed by SH eigenvector analyses of daily 500 m maps in winter (Rogers and van Loon, 1982). The second eigenvector shows a dipole structure across the Andes and a farther eastward extension of these alternating positive and negative anomalies toward the Indian Ocean revealing a wavelength of 80°–120° longitude.

c. Summer teleconnections

Unfiltered and band-pass filtered correlation matrices of SH summer and winter seasons can hardly be distinguished (Fig. 2, lower half-matrix). However, the low-pass filtered correlation coefficients in summer (Fig. 2b) are reduced in comparison with the winter seasons and, therefore, not significant. Although no summertime low-pass features are statistically significant, one major pattern will be discussed, because it also appears in the unfiltered correlation matrix: the transpolar teleconnection. It changes its position from 40°W and 150°E in winter to 70°W and 160°E in summer. The related summer composites (not shown) are similar to those in winter but the area south of Australia and New Zealand (90°E to 180°E), which is affected by the transpolar teleconnection, has broadened. Quite similar to the TPI summer and winter patterns is the zonal distribution of the a_3-index defined by Streten (1980) from surface pressure data of the period 1972–77. This index marks the longitudinal distribution of the latitude, at which the mean surface pressure field poleward of the subtropical high pressure cells is $\leqslant$1015 mb.

d. Zonal wavenumber 3

A wavenumber 3 pattern (presented by negative correlation extrema) may be inferred from some one-point correlation profiles. If low-pass filtered daily geopotentials are considered (Fig. 2), the base point $\lambda = 90°\mathrm{W}$ shows negative correlation maxima with 150°W (which is not significant), 40°W, 40°E. They indicate zonal wave lengths of 110°, 80° and 170° longitude, i.e., wavenumbers between 2 and 4. Furthermore, correlations with the base point $\lambda = 140°\mathrm{E}$ reveal a similar pattern (when moving upward and the right in Fig. 2). Although these correlation values are reduced, the positions of the minima remain at 40°E, 40°W, 150°W. These positions of negative correlations are in some agreement with those found by Mo and White (1985, Fig. 4c). In both data sets one notices the low correlation values over the Pacific after removing each year's annual cycle.

Teleconnections are commonly related to low-pass filtered data sets from which the activity of individual storms has been eliminated. However, storm tracks are revealed by band-pass filtered data sets defining a large-scale and longer-term process. In this sense they are also regarded as a zonal teleconnection pattern:

e. Storm tracks

The band-pass filtered correlation half-matrices (Fig. 2a, b) show about five negatively correlated bands (subdiagonals) parallel to the main diagonal. These are

troughs or ridges related to the 5–10 day periods which are a distance of 30° longitude apart. Spectral densities of the corresponding wavenumber-frequency analyses attain high values in the same domain (Fraedrich and Kietzig, 1983; Salby, 1982), but in a zonally averaged sense. However, the correlation matrix provides a regional differentiation. There are zones of high and reduced (negative) correlations between base points (on the main diagonal) and their neighbors (on the adjacent subdiagonal). Strong negative correlations—they occur between troughs and ridges—are attached to base points on the Indian Ocean from 20° to 110°E, across the South Atlantic (60°W to 10°E) and across the South Pacific from 120° to 180°E. These areas coincide with variance maxima of geopotential height fluctuations (Kietzig, 1983; Trenberth, 1981, 1982) and correspond with the regions of the major storm tracks and jet stream systems of the SH midlatitudes. Summer correlations show similar structures but with less intensity, in particular, over the Indian and Atlantic Oceans.

4. Zonal-time lag correlation: Propagating waves and stationary wave trains

Time lagged zonal cross correlations of geopotential height anomalies are introduced in addition to the zonal correlation matrix. They provide further insight into the time development of teleconnection patterns occurring on shorter (band-pass filtered) and longer (low-pass filtered) periods. Therefore, time lag correlation profiles along 50°S are analyzed. They are centered at $\lambda = 0°$; i.e., downstream of the Atlantic leg of both SAM- and TPI teleconnections (Fig. 4).

Band-pass filtered lag-correlations reveal similar patterns for various seasons and base points (only $\lambda = 0°$ has been selected for presentation, Fig. 4). Correlation maxima or minima move about 10° longitude eastward, if the time lag (of the eastward neighbors of the base point) is increased by multiples of $\Delta t = 1$ day. This yields a phase velocity of 10° per day or 7 to 8 m s^{-1}. The zonal distance between correlation extrema corresponds to a wavelength of 70–80° longitude; i.e., a wavenumber 5 dominates the lag correlation profile along the latitude circle. The wavenumber-frequency spectra averaged over five SH winters produce a peak at medium-scale disturbances, which are associated with wavenumber 5 and phase velocity of 6 m s^{-1} (Fraedrich and Kietzig 1983).

Low-pass filtered lag correlations are deduced by increasing the time lag of grid points eastward of the base point $\lambda = 0°$ by multiples of $\Delta t = 4$ days (Fig. 4). The correlation profiles reveal waves with lengths of about 90° longitude which remain stationary and do not show zonal motion. However, the correlation coefficients which relate the base point ($\lambda = 0°$E) with eastward troughs and ridges increase with increasing time lag, but the westward ones decrease. More specifically, the stationary wave train has four alternating correlation extrema from the South Atlantic to the Indian Ocean (50°W, 0°E, 40°E, 90°E). After 4 and 8 days the first two correlation extrema decrease, the third one increases but less than the fourth. This suggests an energy dispersion along wave trains which emerge from the center of action (i.e., the Atlantic) toward the east. The wave train structure can be identified over about two wavelengths. We observed that this wave train retains its shape and translates eastward when the base point is shifted in this direction. Thus correlation patterns of similar wavelength behave differently at the same base point ($\lambda = 0°$): There is eastward propagation of short period disturbances and energy dispersion toward the east within a stationary wave train, which is related to long periods. It should be noted that the corresponding summer correlations do not show this distinct behavior.

a. A longitude–time lag correlation diagram

More information can be gained from modifying the traditional longitude-time (Hovmöller) diagram of the 500 mb geopotential. In Hovmöller's method geopotential heights of the 500 mb surface along a latitude circle are plotted on the horizontal axis and time increases downward. An example for a SH winter is presented in Fraedrich and Kietzig (1983, Fig. 3) which indicates the downstream development of SH midlatitude disturbances; phase speeds and wavelengths of the traveling troughs can also be estimated. Hovmöller's method is modified to longitude-time lag correlation diagrams at a given base point in the South Atlantic. These longitude-time lag correlations (Fig. 5) display phase- and group velocities (i.e., propagation of wave packets) and the associated wavelength.

The diagram constructed from the band-pass filtered data set (Fig. 5, top) is centered at $\lambda = 0°$E. It reveals a zonal wavelength of 70° to 80° longitude measured between every second zero-correlation contour line (dotted). The zonal phase speed of 10° per day is determined by the slope of maximum positive or negative correlation coefficients. This value is slightly smaller than the phase speed of 12.5° per day, which can be deduced from Blackmon et al. (1984, Fig. 1); they used correlation analyses of the band-pass filtered twice-daily 500 mb geopotential over the North Pacific during winter centered on 40°N, 160°E. The zonal group velocity of 50° per day is the slope of the line which connects the correlation maximum in the center (surrounded by dashed contours) with the neighboring correlation minima (surrounded by full contours) which are related to positive and negative time lags. Other base points and the zonal average (not shown) provide essentially the same values for wavelength,

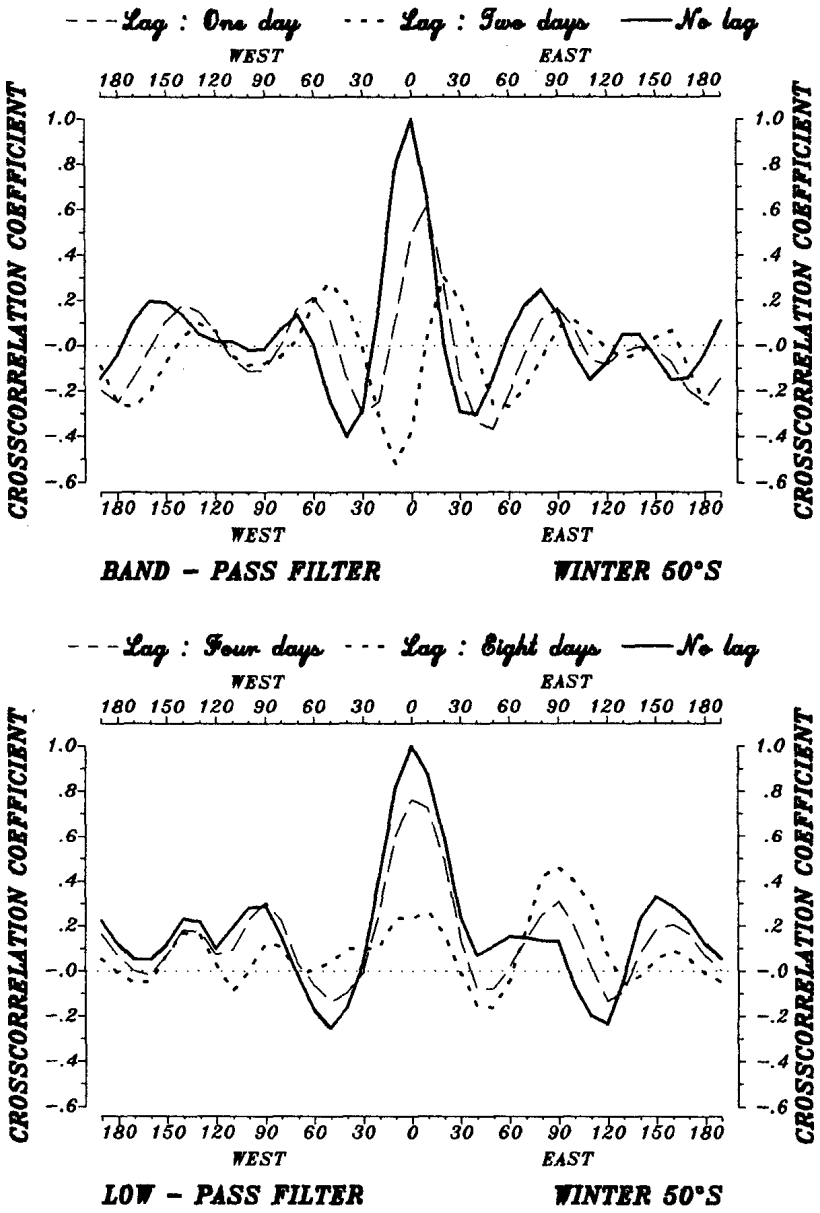

FIG. 4. Time lag-correlations of band- and low-pass filtered geopotential height deviations along 50°S centered at $\lambda = 0°$ during winter (top); band-pass filter with lags of 1 day shows eastward propagating waves (bottom); low-pass filter with lags of 4 days shows a stationary wave train with eastward energy dispersion.

phase- and group velocity. Seasonal differences can hardly be distinguished. A nondivergent progressive Rossby wave of the same wavelength (or wavenumber k), phase- and group velocity ($c_{p,g} = u \mp \beta k^{-2}$) would require a zonal current of $u \sim 27.5$–$32.5°$ per day or $u \sim 22.5$ m s^{-1}. This is in agreement with observed climatological mean values for winter (e.g., Trenberth, 1982, Fig. 1).

The low-pass filtered correlation diagram (Fig. 5, bottom) is also centered at $\lambda = 0°$E. It is dominated by a stationary wave train with a wavelength of 90° to 100° longitude. The wave packet encounters a group velocity of $\sim 10°$ per day. This can be estimated if one follows the series of correlation extrema which alternate their sign when changing from negative to positive time lags.

5. Summary and discussion

This study extends the statistical and wavenumber-frequency analysis of an uncommon SH data set by

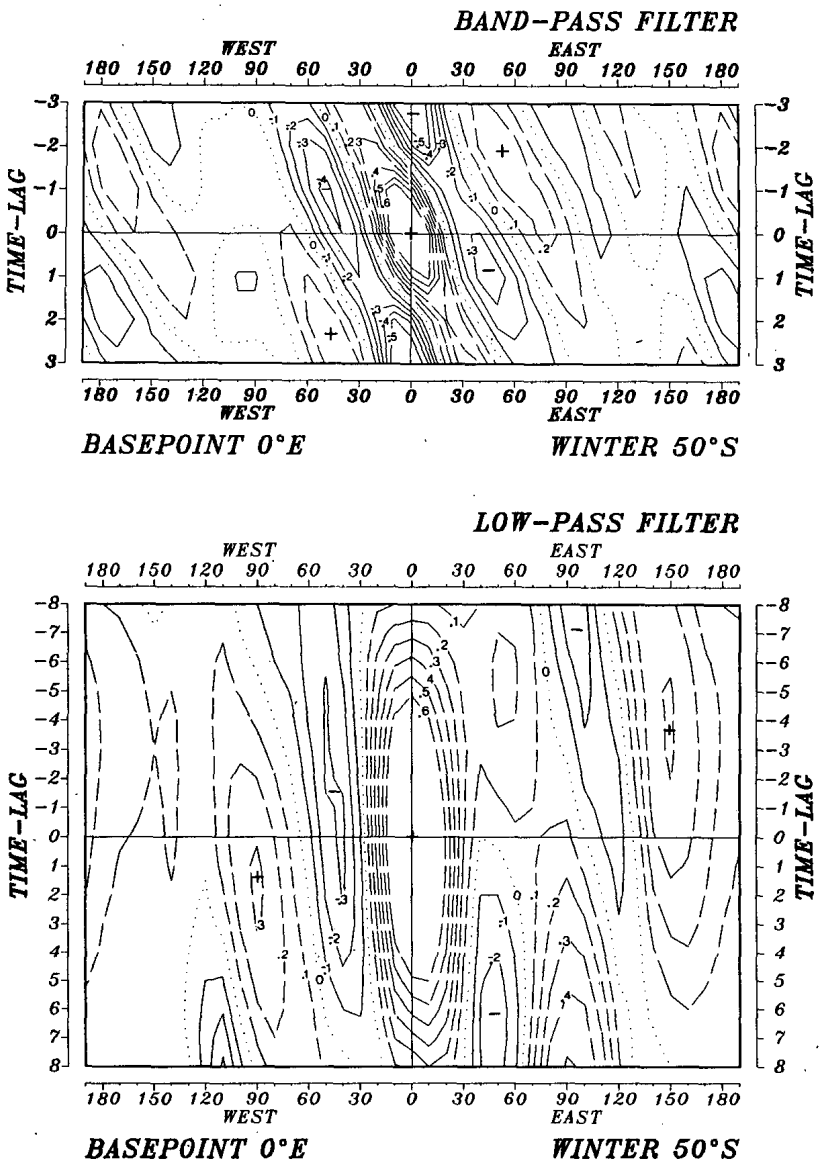

FIG. 5. Longitude–time lag correlation diagrams of band-pass (top) and low-pass (bottom) filtered 500 mb geopotential heights along 50°S during winter, centered at the base point $\lambda = 0°E$. Positive, negative and zero correlations are defined by dashed, full and dotted contour lines, respectively.

applying simultaneous and time lag-correlation statistics to band- and low-pass filtered geopotentials along 50°S. Due to the Southern Hemisphere zonality it is sufficient for many purposes to analyze zonal data sets on a representative latitude circle. Some results of the analysis may be summarized:

• Southern Hemisphere midlatitude teleconnections are deduced from matrices of simultaneous cross correlations of the low-pass filtered 500 mb geopotential along 50°S: a South American anomaly, the transpolar teleconnection, and a wavenumber 3 pattern (with contributions from wavenumbers 2 and 4). Representative correlation timescales, associated with the correlation matrices, are estimated. These correlation matrices provide a suitable mean for comparing and testing the low-frequency variability of general circulation models with observations.

• Modified Hovmöller diagrams, which present zonal-time lag-correlations (for a selected base point), are constructed using band- and low-pass filtered geopotentials along 50°S. They display wavelengths, phase- and group velocities. The short period fluctuations (of the band-pass filtered geopotentials) can be related to the synoptic disturbances of the SH midlatitudes. They reveal a zonal wavelength of 60° longitude, a phase velocity of ~10° per day and a group velocity of ~50° per day. The long period fluctuations (of the low-pass filtered geopotentials) display a zonal wave train (for

base points over the mid South Atlantic) with a wavelength of 90° to 100° longitude and almost no phase change. It shows an eastward energy dispersion which can be associated with a group velocity of 5 to 10 m s^{-1}; the structure is kept approximately over two wavelengths. These wave trains seem to resemble those discussed by Blackmon et al. (1984a) associated with the 10 to 30 day time scale. This is in agreement with the low-pass filtered correlation time scale ($\bar{T}_0 \sim 15$ to 20 days; see Appendix). They are documented in the NH, where they are organized in more zonally oriented waveguides originating in the jet entrance regions. They retain their shape and simply translate eastward with the base point.

Acknowledgment. This note has been written during a visit (K.F.) at the Joint Institute for the Study of the Atmosphere and Ocean (JISAO) and the Department of Atmospheric Sciences, University of Washington, Seattle. Stimulating discussions and the support of J. M. Wallace are gratefully acknowledged. Thanks are due to Ms. S. Parker and Ms. M. Scholz for typing.

APPENDIX

Estimating the Significance of Correlation Coefficients

Autocorrelations $r_{\lambda,L}$ determine the time lag L-correlation profiles at each gridpoint λ. They allow an estimate of a time scale T_0 which denotes the time between effectively independent observations. Referring to correlations between the time series $z^*(\lambda, t)$ and $z^*(\lambda + m\Delta\lambda, t)$, a time scale (Bartlett, 1935; see also Trenberth 1984, 1985 for some details) is defined by

$$T_0(\lambda, \lambda + m\Delta\lambda) = 1 + 2 \sum_{L=1}^{N} (1 - L/N)(r_{\lambda,L})(r_{\lambda+m,L}).$$

Assuming red noise, i.e., a first order autoregressive process (AR), the autocorrelations at lag L are then estimated by $r_L = r_1{}^L$. Averaging the correlation time scale matrix based on red noise, $T_0(\lambda, \lambda + m\Delta\lambda)$, gives a representative mean value $\bar{T}_0$ for the 50°S latitude circle. For the unfiltered, band-, and low-pass filtered data sets one obtains the following average time scales:

$$\bar{T}_0 = \begin{cases} (1.7; 1.8; 18.8) & \text{days for winter} \\ (1.5; 1.6; 17.4) & \text{days for summer.} \end{cases}$$

To evaluate the significance of the correlation coefficients it should be noted that the appropriate degrees of freedom are defined by independent data; i.e., the number of observations is reduced by the factor sampling time Δt/time scale T_0. Thus one obtains the following 95% significant correlation coefficients for the unfiltered, band- and low-pass filtered data sets: $r_u = 0.11$, $r_{bp} = 0.11$, $r_{lp} = 0.44$ for winter; $r_u = 0.10$, $r_{bp} = 0.10$, $r_{lp} = 0.34$ for summer. They define average values which are representative for the complete correlation matrix and indicated on the legend attached to it. Individual T_0-values do not exceed $2\bar{T}_0$; they still lead to the same 95% significant bounds as given by the legends of Fig. 1 (referring to unfiltered and band-pass filtered correlations) or Fig. 2 (for low-pass filtered correlations). The same significance levels apply to the correlations shown in Figs. 4 and 5.

REFERENCES

Bartlett, M. S., 1935: Some aspects of the time-correlation problem in regard to tests of significance. *J. Roy. Stat. Soc.*, **98,** 536–543.

Blackmon, M. L., 1976: A climatological spectral study of the 500 mb geopotential height of the Northern Hemisphere. *J. Atmos. Sci.*, **33,** 1607–1623.

——, Y.-H. Lee and J. M. Wallace, 1984a: Horizontal structure of 500 mb height fluctuations with long, intermediate and short time scales. *J. Atmos. Sci.*, **41,** 961–979.

——, ——, —— and H.-H. Hsu, 1984b: Time variation of 500 mb height fluctuations with long, intermediate and short time scales as deduced from lag-correlation statistics. *J. Atmos. Sci.*, **41,** 981–991.

Bradley, J. V., 1968: *Distribution-free Statistical Tests,* Prentice-Hall, 105–117.

Coughlan, M. J., 1983: A comparative climatology of blocking action in the two hemispheres. *Aust. Meteor. Mag.*, **31,** 3–13.

Dole, R. M., 1983: Persistent anomalies of the extratropical Northern Hemisphere wintertime circulation. Large-scale dynamical processes in the atmosphere, B. F. Hoskins and R. P. Pearce, Eds., Academic Press, 95–110.

Fraedrich, K., and E. Kietzig, 1983: Statistical analysis and wavenumber-frequency spectra of the 500 mb geopotential along 50° South. *J. Atmos. Sci.*, **40,** 1037–1045.

Hamilton, K., 1983: Aspects of wave behavior in the mid- and upper troposphere of the Southern Hemisphere. *Atmos.-Ocean,* **21,** 40–54.

Hartmann, D. L., 1976: The structure of the stratosphere in the Southern Hemisphere during late winter 1973 as observed by satellite. *J. Atmos. Sci.*, **33,** 1141–1154.

——, A. J. Simmons and D. G. Andrews, 1977: Energy dispersion in a barotropic atmosphere. *Quart. J. Roy. Meteor. Soc.*, **103,** 553–567.

Kietzig, E., 1984: Statistical analysis of the 500 mb geopotential along 50° North and South: Moments and time scales. *Meteor. Rundsch.*, **37,** 11–116.

Mann, H. B., and D. R. Whitney, 1947: On a test of whether one of two random variables is stochastically larger than the other. *Ann. Math. Stat.*, **18,** 50–60.

Mechoso, C. R., and D. L. Hartmann, 1982: An observational study of travelling planetary waves in the Southern Hemisphere. *J. Atmos. Sci.*, **39,** 1921–1935.

Mo, K. C., and G. H. White, 1985: Teleconnections in the Southern Hemisphere. *Mon. Wea. Rev.*, **113,** 22–37.

NOTOS, 1964–1970: Historical weather charts for the Southern Hemisphere. *Atmospheric Project Southern Hemisphere,* Pretoria, South African Weather Bureau, 13–19.

Pittock, A. B., 1980: Patterns of climatic variation in Argentina and Chile—I. Precipitation 1931–1960. *Mon. Wea. Rev.*, **108,** 1347–1361.

——, 1984: On the reality, stability, and usefulness of southern hemisphere teleconnections. *Aust. Meteor. Mag.*, **32,** 75–82.

Randel, W. F., 1985a: An observational study of medium-scale wave

dynamics in the Southern Hemisphere summer. Part I: Wave structure and energetics. *J. Atmos. Sci.*, **42,** 1172–1188.

——, 1985b: An observational study of medium-scale wave dynamics in the Southern Hemisphere summer. Part II: Stationary-transient wave interference. *J. Atmos. Sci.*, **42,** 1189–1197.

——, and F. L. Stanford, 1983: Structure of medium-scale atmospheric waves in the Southern Hemisphere summer. *J. Atmos. Sci.*, **40,** 2312–2318.

Rogers, J. C., and H. van Loon, 1982: Spatial variability of sea level pressure and 500 mb height anomalies over the Southern Hemisphere. *Mon. Wea. Rev.*, **110,** 1375–1392.

Salby, M. L., 1982: A ubiquitous wavenumber-5 anomaly in the Southern Hemisphere during FGGE. *Mon. Wea. Rev.*, **110,** 1712–1720.

Streten, N. A., 1980: Some synoptic indices of the Southern Hemisphere mean sea level circulation 1972–77. *Mon. Wea. Rev.*, **108,** 18–36.

Taljaard, J. J., and H. van Loon, 1960: The construction of 500 mb contour maps over the Southern Ocean. *Antarctic Meteorology,* Pergamon, 96–114.

——, and ——, 1964: Southern hemisphere weather maps for the International Geophysical Year. *Bull. Amer. Meteor. Soc.*, **45,** 88–95.

Trenberth, K. E., 1981: Observed Southern Hemisphere eddy statistics at 500 mb: Frequency and spatial dependence. *J. Atmos. Sci.*, **38,** 2585–2605.

——, 1982: Seasonality in Southern Hemisphere eddy statistics at 500 mb. *J. Atmos. Sci.*, **39,** 2507–2520.

——, 1984: Some effects of finite sample size and persistence on meteorological statistics. Part I: Autocorrelations. *Mon. Wea. Rev.*, **112,** 2359–2368.

——, 1985: Persistence of daily geopotential heights over the Southern Hemisphere. *Mon. Wea. Rev.*, **113,** 38–53.

——, and K. C. Mo, 1985: Blocking in the Southern Hemisphere. *Mon. Wea. Rev.*, **113,** 3–21.

van Loon, H., 1956: Blocking action in the Southern Hemisphere. *NOTOS,* **5,** 171–177.

Wallace, J. M., and D. S. Gutzler, 1981: Teleconnections in the geopotential height field during the Northern Hemisphere winter. *Mon. Wea. Rev.*, **109,** 784–812.

——, and H.-H. Hsu, 1983: Ultra-long waves and two-dimensional Rossby waves. *J. Atmos. Sci.*, **40,** 2211–2219.